Vol. 76: 49–69, 2015
doi: 10.3354/ame01767

AQUATIC MICROBIAL ECOLOGY
Aquat Microb Ecol

Published online September 23

FREE ACCESS

Winter–spring transition in the subarctic Atlantic: microbial response to deep mixing and pre-bloom production

Maria Lund Paulsen[1,2,*], Karen Riisgaard[2], T. Frede Thingstad[1], Mike St. John[2], Torkel Gissel Nielsen[2]

[1]Marine Microbiology Research Group, Department of Biology, University of Bergen, Thormøhlensgate 53A/B, 5020 Bergen, Norway

[2]National Institute of Aquatic Resources, DTU-Aqua, Section for Ocean Ecology and Climate, Technical University of Denmark, Jægersborg Allé 1, 2920 Charlottenlund, Denmark

ABSTRACT: In temperate, subpolar and polar marine systems, the classical perception is that diatoms initiate the spring bloom and thereby mark the beginning of the productive season. Contrary to this view, we document an active microbial food web dominated by pico- and nanoplankton prior to the diatom bloom, a period with excess nutrients and deep convection of the water column. During repeated visits to stations in the deep Iceland and Norwegian basins and the shallow Shetland Shelf (26 March to 29 April 2012), we investigated the succession and dynamics of photosynthetic and heterotrophic microorganisms. We observed that the early phytoplankton production was followed by a decrease in the carbon:nitrogen ratio of the dissolved organic matter in the deep mixed stations, an increase in heterotrophic prokaryote (bacteria) abundance and activity (indicated by the high nucleic acid:low nucleic acid bacteria ratio), and an increase in abundance and size of heterotrophic protists. The major chl *a* contribution in the early winter–spring transition was found in the fraction <10 µm, i.e. dominated by pico- and small nanophytoplankton. The relative abundance of picophytoplankton decreased towards the end of the cruise at all stations despite nutrient-replete conditions and increasing day length. This decrease is hypothesised to be the result of top-down control by the fast-growing population of heterotrophic protists. As a result, the subsequent succession and nutrient depletion can be left to larger phytoplankton resistant to small grazers. Further, we observed that large phytoplankton (chl *a* > 50 µm) were stimulated by deep mixing later in the period, while picophytoplankton were unaffected by mixing; both physical and biological reasons for this development are discussed herein.

KEY WORDS: Microbial food web · Winter–spring transition · Deep mixing · Picophytoplankton · Nanophytoplankton · Bacteria · Heterotrophic nanoflagellates · Microzooplankton · Subarctic Atlantic

INTRODUCTION

Much of our conceptual understanding of the marine pelagic food web originates from the pioneer work of Sverdrup (1953), Cushing (1959) and Steele (1974). This understanding was based on coarse-meshed samplers, e.g. continuous plankton recorder surveys and vertical net hauls, and used to describe the seasonality of northern marine ecosystems and inspired generations of marine researchers. However, little attention was paid to the role of microbial communities, in part due to the difficulty in sampling this component of the food web. With the advent of suitable techniques, the microbial loop has been recognised to play a fundamental role in the flux of carbon and nutrients in marine ecosys-

*Corresponding author: maria.l.paulsen@uib.no

tems (Pomeroy 1974, Sorokin 1977, Azam et al. 1983). Thus, the importance of the heterotrophic components of the microbial loop became recognised (Williams 1981); however, the role of photosynthetic picophytoplankton in northern ecosystems still received little attention. This was due to the fact that sampling efforts traditionally have been focused on the spring bloom period because the new production of larger-celled species in this period has a strong link to mesozooplankton and fish production (Sverdrup 1953, Steele 1974, Braarud & Nygaard 1978). During the spring bloom, the relative abundance of picophytoplankton is low (Li et al. 1993) when compared to oligotrophic subtropical waters (Agawin et al. 2000). The spring diatom bloom, however, is a short-term feature of the system, with smaller phytoplankton and their associated grazers dominating for the majority of the year. The microbial food web, including picophytoplankton, has received more attention in recent years in northern systems (Søndergaard et al. 1991, Joint et al. 1993, Sherr et al. 2003, Irigoien et al. 2005, Tremblay et al. 2009, Seuthe et al. 2011a,b).

In winter, the water column is characterized by high turbulent mixing, deep convection (Backhaus et al. 1999) and low irradiance. During this period, phytoplankton concentrations are dispersed (Li 1980), and the major mesozooplankton grazer, *Calanus finmarchicus*, is in diapause at depth (Hirche 1996). The onset of the bloom is affected by several physical factors, which have been thoroughly described, including a shoaling of deep convection (Taylor & Ferrari 2011), periods below the threshold of critical turbulence (Huisman 1999), eddy-driven stratification (Mahadevan et al. 2012) and irradiance (i.e. the critical depth model; Sverdrup 1953). Grazing by microzooplankton (MZP) has also been suggested to play a major role in the bloom development. Behrenfeld (2010) and Behrenfeld & Boss (2014) hypothesised that the increase in phytoplankton biomass in the North Atlantic during the winter–spring transition could be the result of a decoupling of the MZP grazers from their phytoplankton prey during mixed layer deepening (the dilution–recoupling hypothesis). There has been controversy as to the mechanisms controlling the onset of the bloom, resulting in a publication by Lindemann & St. John (2014) presenting a conceptual model of the interplay of these abiotic and biotic mechanisms. However, no attempt has been made to investigate the photosynthetic planktonic community composition and grazing dynamics in the subarctic Atlantic during deep convection.

Here, we shift the focus from the diatom spring bloom to the microbial community found during the winter–spring transition and evaluate the relative contributions of pico- and nanophytoplankton in the subarctic North Atlantic prior to the bloom. We investigate the succession of both photosynthetic and heterotrophic plankton components and evaluate a central hypothesis behind bloom formation in well-mixed waters, i.e. the decoupling of the heterotrophic protists from the phytoplankton community during deep mixing. In addition to the *in situ* observations presented here, an experimental approach was applied to study the microbial interactions in detail (e.g. estimation of growth and grazing rates); these are presented in K. Riisgaard et al. (unpubl.)

MATERIALS AND METHODS

Sampling site and hydrography

The study was conducted from 26 March to 29 April 2012 during a cruise aboard the RV 'Meteor' (cruise no. 87) coordinated by the University of Hamburg, Germany. The study focused on 3 stations located in the subarctic North Atlantic, representing different hydrographical regimes: 2 stations on the edge of the deep basins north and south of the Greenland–Scotland Ridge in the Norwegian Basin (1300 m) and Iceland Basin (1350 m), respectively, and 1 station on the shallow Shetland Shelf (160 m) (Fig. 1). Each station was revisited at 8 to 14 d intervals following a route circling the Faroe Islands. During each visit, vertical profiles of temperature, salinity and photosynthetically active radiation (PAR) were performed using a Sea-Bird CTD (SBE 9 plus) with an attached rosette of 10 l Niskin bottles.

Photic zone depth was defined as 0.1% of incident PAR measured at 5 m (Jerlov 1968). The depth of the mixed layer was identified as a decrease of 0.2°C from surface (10 m) temperatures (de Boyer Montégut et al. 2004), evaluated to be the most appropriate definition for high latitude regions where deep convection can occur.

Sampling depths were chosen based on water column structure and covered the full water column, with the highest resolution within the mixed layer. During each visit to the stations, 3 CTD profiles were taken within a time frame of 20 to 36 h to capture the temporal dynamics (i.e. data presented from each visit in the following discussion is an average of 3 profiles). Samples were collected to provide data on the abundance of microbial components, including

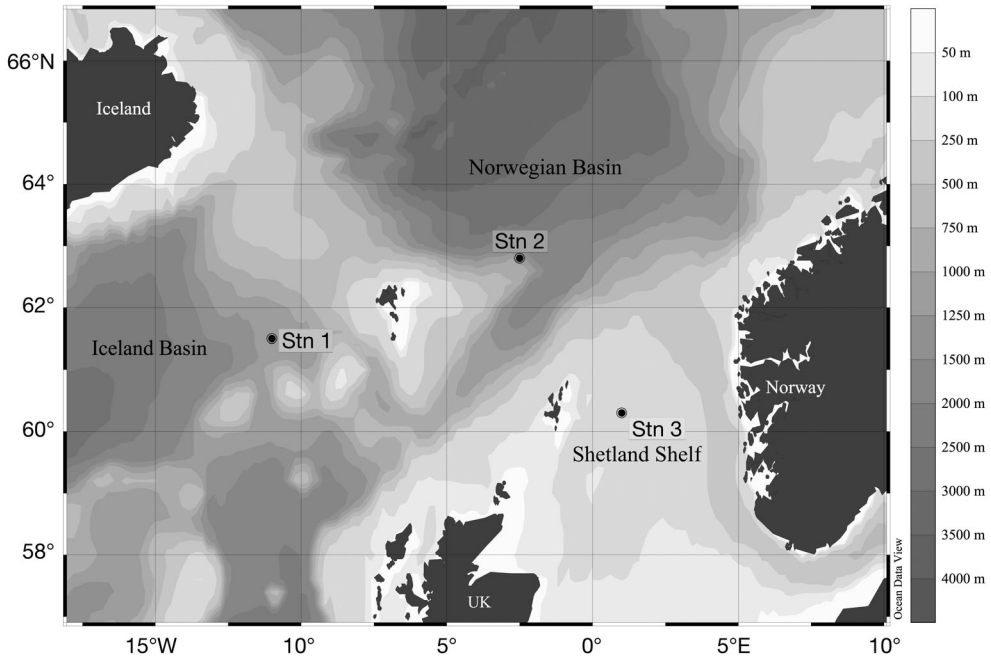

Fig. 1. Study area. Stn 1: 1350 m deep station in the Iceland Basin (61.5° N, 11° W); Stn 2: 1300 m deep station in the Norwegian Basin (62.8° N, 2.5° W); Stn 3: 160 m deep station on the Shetland Shelf (60.3° N, 1° E)

virus-like particles (hereafter referred to as virus), heterotrophic prokaryotes (Archaea and bacteria, hereafter referred to as bacteria), small (<10 µm) phytoplankton, unidentified heterotrophic nanoflagellates (HNF) and larger (>10 µm) ciliates and dinoflagellates (i.e. MZP) as well as chl *a*, nutrients and dissolved organic carbon and nitrogen (DOC and DON, respectively). The sampling of bacteria, viruses, small phytoplankton and total chl *a* was about twice as frequent as sampling of the more analytically time-consuming fractionated chl *a* and heterotrophic protists.

Nutrients, organic matter and chl *a*

Nitrate and nitrite (NO_3+NO_2), phosphate (PO_4) and silicic acid (H_4SiO_4) were measured on a Skalar Sanplus segmented-flow autoanalyser, following procedures outlined by Wood et al. (1967) for NO_3+NO_2, Murphy & Riley (1962) for PO_4 and Koroleff (1983) for the determination of H_4SiO_4.

Total organic carbon (TOC) in unfiltered seawater was analyzed by high-temperature combustion using a Shimadzu TOC-V_{CSH}. Standardization was achieved using potassium hydrogen phthalate. Calibration was performed using deep seawater and low carbon reference waters as provided by the Hansell consensus reference materials (CRM) program and performed every sixth analysis to assess the day-to-day and instrument-to-instrument variability. The precision of TOC analyses was ~1 µmol kg^{-1}, with a coefficient of variation of 2 to 3%. Concentration of total nitrogen was determined simultaneously by high temperature combustion using a Shimadzu TNM1 attached to the Shimadzu TOC-V. Total organic nitrogen (TON) was calculated by subtracting total inorganic nitrogen (NO_3+NO_2) measured from parallel nutrient samples on board. As ammonium concentrations were negligible throughout the cruise, with a mean of 0.18 µM ± 0.5, n = 400, within the upper mixed layer (J. Jacob unpubl.), these were not included in the total inorganic nitrogen pool. Non-purgeable dissolved nitrogen compounds are combusted and converted to nitric oxide, which when mixed with ozone chemiluminesces for detection by a photomultiplier. Both measurements were quality controlled using CRMs distributed to the international community (Hansell 2005). The CRMs were analyzed at regular intervals during each analytical day (Hansell 2005). As the difference between TOC and DOC is minor in northern systems during non-bloom situations (Anderson 2002), we use the term DOC; for organic nitrogen, we use DON instead of TON.

Chl *a* concentrations were determined from 100 to 1000 ml samples and size fractionated on Whatman GF/F filters (0.7 µm pore size), 10 and 50 µm mesh; each fractionation treatment was triplicated. Filters were extracted in 5 ml of 96% ethanol for 12 to 24 h (Jespersen & Christoffersen 1987). Chl *a* concentrations were measured before and after addition of 1 drop of acid (1 M HCl) on a TD-700 Turner fluorometer, which was calibrated against a chl *a* standard.

Enumeration of bacteria, viruses and protists

Bacteria, viruses, small phytoplankton and HNF were enumerated using a FACSCalibur (Becton Dickinson) flow cytometer and analysed using CellQuest software.

Samples for phytoplankton and bacteria were fixed with glutaraldehyde (final conc. 0.5%) for 30 min in the dark at 4°C, while HNF were fixed with glutaraldehyde (final conc. 0.43%) for 2 h. Thereafter, all samples were flash frozen in liquid nitrogen and stored at −80°C until further analysis (within 4 mo).

Small phytoplankton were analysed directly after thawing for 5 min at a flow rate of 60 to 70 µl min^{-1}. Groups of picoeukaryotes, *Synechococcus* and small and large nanophytoplankton were discriminated on the basis of their side scatter (proportional to cell size) and red fluorescence (Fig. 2A) as in Larsen et al. (2004). Further, the mean red fluorescence per cell within each group was recorded.

For the enumeration of bacteria and viruses, samples were diluted (5- and 10-fold) with 0.2 µm filtered TE buffer (Tris 10 mM, EDTA 1 mM, pH 8), stained with a green fluorescent nucleic acid dye (SYBR Green I; Molecular Probes) and kept for 10 min at 80°C in a water bath to provide optimal staining of viruses (Marie et al. 1999). Samples were counted for 1 min at a flow rate of ~30 µl min^{-1} and discriminated on the basis of their side scatter and green fluorescence (Fig. 2B). As reference, yellow-green fluorescent beads of 2 µm diameter (FluoSpheres® Molecular Probes carboxylate-modified microspheres) were added. Bacteria are often found to group into 2 distinct clusters of high and low green fluorescence (Sherr et al. 2006, Huete-Stauffer & Morán 2012). As division was clear in current samples (Fig. 2B), the total bacteria counts were divided into subgroups of low nucleic acid (LNA) and high nucleic acid (HNA).

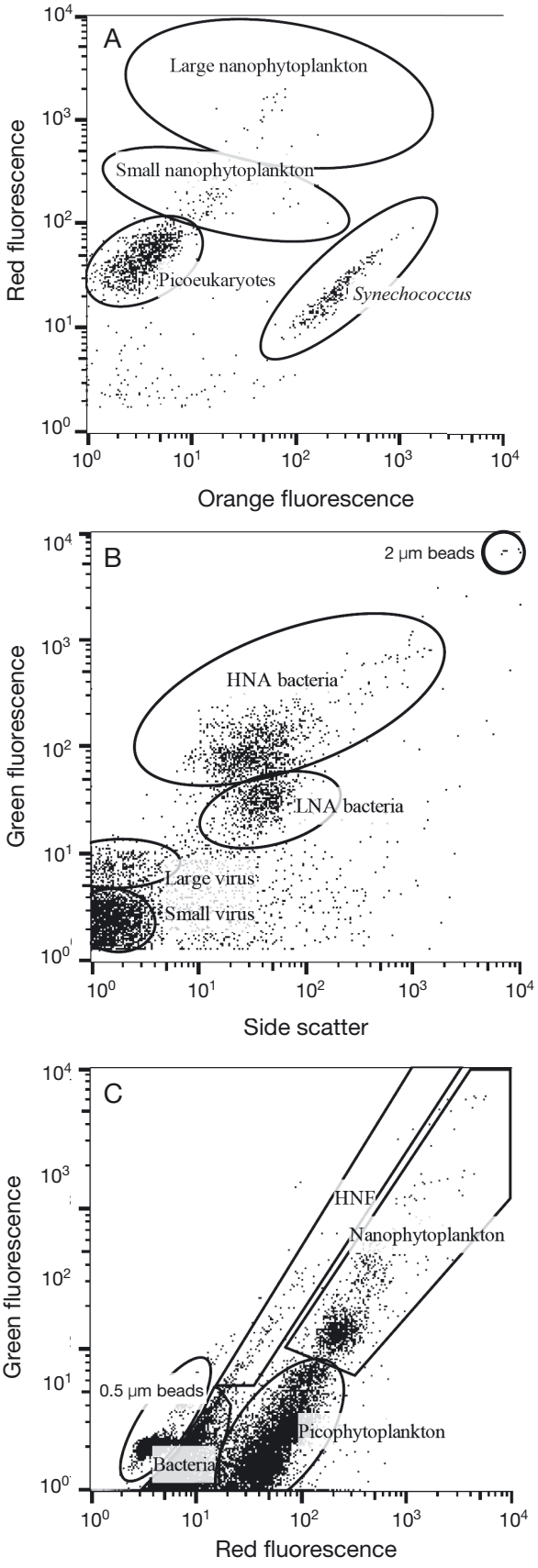

Fig. 2. Biparametric flow cytometry plots with the applied grouping of the different microbial groups. (A) Populations of photosynthetic picoeukaryotes, *Synechococcus* sp. and 2 size groups of nanoflagellates distinguished on a plot of red fluorescence vs. orange fluorescence. (B) Heterotrophic bacteria and viruses as distinguished on a plot of green fluorescence vs. side scatter. The group of high nuclei acid (HNA) bacteria expresses higher fluorescence than the low nuclei acid (LNA) bacteria, yet another gate for total bacteria covered both HNA and LNA; 2 µm fluorescent reference beads appear in the right upper corner of the plot. (C) Heterotrophic nanoflagellates (HNF) are distinguished from nano-sized phototrophic protists on a plot of red fluorescence vs. green fluorescence. Bacteria and picophytoplankton are found at the bottom of the plot as well as 0.5 µm fluorescent beads (see further explanation in the text)

Table 1. Weighted arithmetic means of measured equivalent spherical diameter (ESD) within the size fractions chosen to represent small and large autotrophic nanoflagellates (ANF), heterotrophic nanoflagellates (HNF), picoeukaryotes and *Synechococcus* sp. as well as the carbon conversion factors used to convert estimates of cell abundance to biomass (pg C cell^{-1}). Dinoflagellates and ciliates are estimated from biovolumes (V) of each individual, and average ESD is therefore not presented. For smaller protist groups, average ESD was measured; for HNF, diameter was estimated by UV epifluorescence microscopy; for small phytoplankton, the weighted arithmetic mean of the diameter was calculated from the abundance within different size intervals using filtration (see further explanation in 'Size and biomass estimation of protists'). The biomass of bacteria is estimated using literature values. –: not measured

Group	Measured ESD (µm)	Carbon conversion (fg C µm^{-3})	Conversion reference	Biomass (pg C cell^{-1})
Dinoflagellates	–	Log (pg C cell^{-1}) = –0.353 + 0.864 log (V)	Menden-Deuer & Lessard (2000)	–
Aloricate ciliates	–	Log (pg C cell^{-1}) = –0.639 + 0.984 log (V)	Putt & Stoecker (1989), modified by Menden-Deuer & Lessard (2000)	–
Loricate ciliates	–	Log (pg C cell^{-1}) = –0.168 + 0.841 log (V)	Verity & Langdon (1984), Menden-Deuer & Lessard (2000)	–
HNF	3.2 ± 0.3	220	Børsheim & Bratbak (1987)	3.80
Bacteria	–	–	Lee & Fuhrman (1987)	0.02
Large ANF	8 ± 0.7	220	Mullin et al. (1966)	58.98
Small ANF	4 ± 0.5	220	Mullin et al. (1966)	7.37
Picoeukaryotes	1.7 ± 0.4	220	Mullin et al. (1966)	0.57
Synechococcus sp.	1.1 ± 0.4	250	Kana & Glibert (1987)	0.17

Samples for HNF were stained with SYBR Green I for 2 to 4 h in the dark at 4°C, and 0.5 µm yellow-green fluorescent beads were added as reference. A 2 ml undiluted sample was analysed, and HNF were discriminated from phototrophic nanoflagellates in bivariate plots of the green fluorescence (from SYBR Green) vs. red fluorescence (from chl *a*) (Fig. 2C), following the method of Zubkov et al. (2007). The samples were measured at a lower flow rate (120 µl min^{-1}) than that used in Zubkov et al. (2007) (180 to 1000 µl min^{-1}); however, the lower flow rate was compensated by longer measuring time, i.e. comparable volumes were measured. With this method, we could not distinguish mixotrophic nanoflagellates.

For enumeration and sizing of larger protists, water samples of 500 ml were gently decanted from the Niskin bottle through a silicon tube into brown glass bottles and fixed in acidic Lugol's solution (final conc. 3%) and kept cool and dark until analysis. To concentrate the samples, 500 ml subsamples were allowed to settle for 48 h in tall cylinders (height: 34.5 cm, diameter: 5 cm) before the upper part of the sample was gently removed by decanting with a silicon tube, leaving 100 ml in the cylinder. All (or a minimum of 300) cells were counted using an inverted microscope (Nikon K18).

Size and biomass estimation of protists

Dinoflagellates and ciliates were identified morphologically and divided into size classes covering 10 µm ranges of equivalent spherical diameter (ESD) starting with 10 to 20 µm. ESD and cell volume are related by $\pi/6 \times ESD^3$ = cell volume. Cell volumes were calculated using appropriate geometric shapes without including the membranelles (tufted arrangements of cilia). The biovolumes were converted to carbon using the volume:carbon conversion factors given in Table 1. Qualitative observations of dominant microphytoplankton families and species were recorded in parallel.

The biomass of pico- and nanoflagellates was estimated based on literature conversion factors (Table 1). Size determinations of the various groups of phytoplankton (picoeukaryotes, *Synechococcus* sp. and small and large nanophytoplankton) were performed by filtering parallel samples through 0.8, 1, 2, 5 and 10 µm polycarbonate filters and counting the filtrate, thereby enumerating the percentage of each group within the given size interval, a method modified from Zubkov et al. (1998).

HNF size was estimated using epifluorescence microscopy. Samples (10 ml) were fixed with glutaraldehyde (final conc. 1%) for 1 h and stored at –80°C. The samples were filtered onto black polycarbonate filters (pore size 0.8 µm), stained with DAPI DNA-specific dye (Porter & Feig 1980) and analysed under a UV epifluorescence microscope (1000×). To ensure that the measured cells were heterotrophic, each cell was crosschecked for red fluorescence. A total of 170 HNF were measured (~30 HNF were measured from both surface and subsurface samples at each station). As there was no sig-

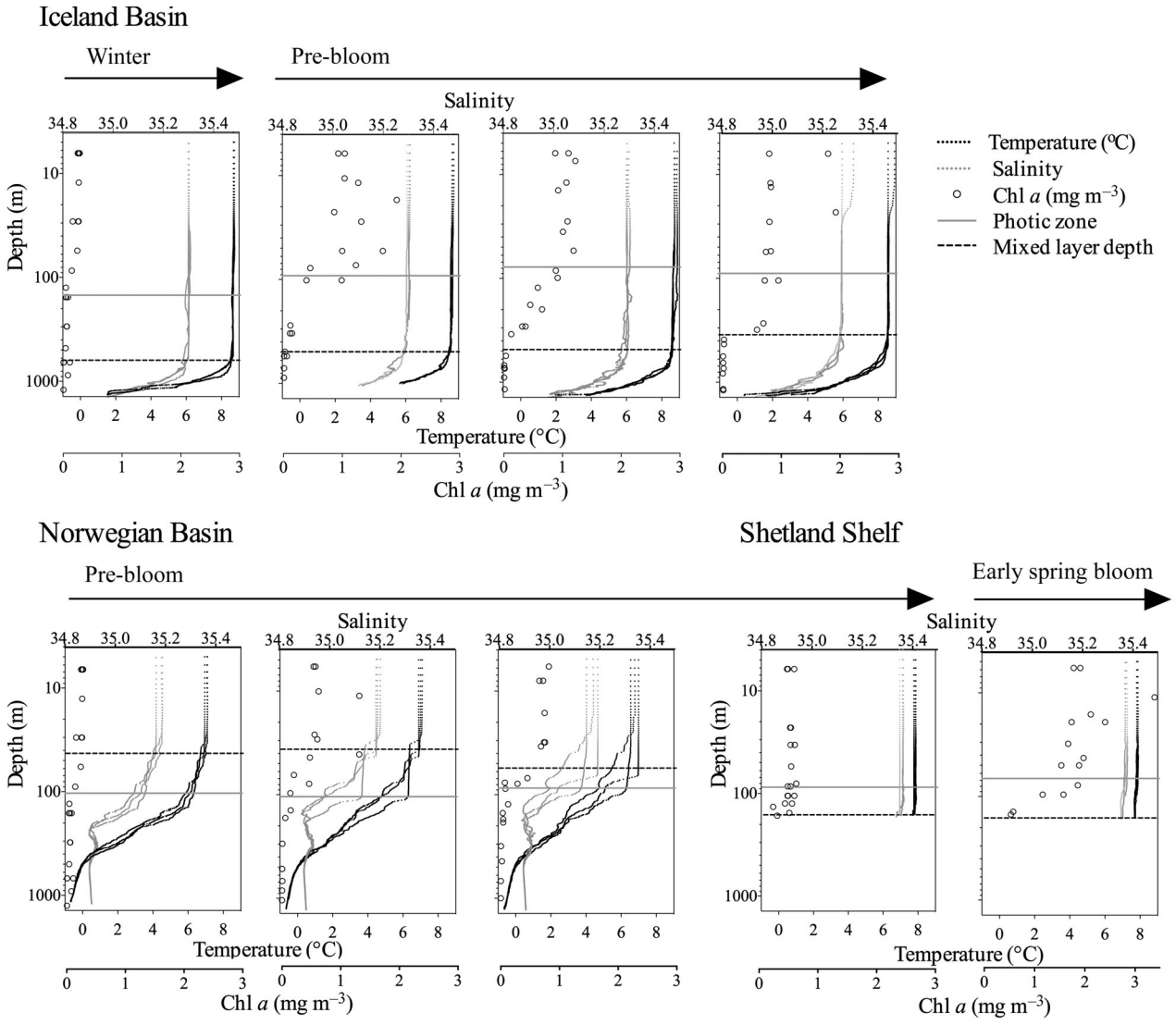

Fig. 3. Vertical profiles (n = 3) of salinity, temperature and total chl *a* (sampled from the chosen sampling depths). All profiles were taken within 20 to 36 h (first visit to the left). Horizontal arrows indicate the seasonal phase. Horizontal black dashed line indicates the mixed layer depth; gray line marks the photic zone

nificant difference between the size measures, a total mean was later used for biomass estimation. For both HNF and groups of small phytoplankton, the abundance within size intervals was converted to the weighted arithmetic averaged size and used for biomass estimation (Table 1).

Integrated values were calculated by trapezoid integration to the bottom, 600 m or the base of the mixed layer (see Figs. 4 & 7). When samples were not available from the exact mixed layer depth (MLD), a curve was fitted between the 2 neighbouring samples and the resulting curve equation used to estimate the value by the base of the mixed layer. The integrated biomass values (mg C m^{-2}) were converted to mg C m^{-3} by dividing by the depth of the mixed layer to enable comparison of the mean integrated biomass within the mixed layer between stations. Data included in the paper are available from the data repository PANGAEA via Paulsen et al. (2014a,b) for abundance measurements of pico- and nanoplankton during RV 'Meteor' cruise no. 87.

RESULTS

Physical regime

Weather during the cruise was generally windy, causing mixing of the upper part of the water column in addition to the winter convection. The deep stations in the Iceland and Norwegian basins were mostly stormy, and on several occasions, winds

reached Beaufort force 10 with sustained periods of Beaufort 8 and wave heights of 3 to 5 m. The day length increased from 11 to 16 h during the cruise.

The deep Iceland Basin station (bottom = 1350 m) deep convection or remnants thereof was evident down to ~600 m but reduced gradually to ~350 m during the study period (MLD = 600 to 344 m) (Fig. 3). Based on the water mass definitions of Blindheim & Østerhus (2005) potential temperature (θ) and salinity, the Iceland Basin consisted mostly of Atlantic Water (θ = 5 to 10.5°C, salinity = 35 to 35.05) reaching >1000 m depth, while Polar Overflow Water (θ < 0.5°C, salinity = 34.88 to 34.93) was observed near the bottom on a few occasions.

The deep Norwegian Basin (bottom = 1300 m) had a persistently shallower mixed layer around ~50 m (MLD = 37 to 56 m). Here, the Atlantic Water was constrained to the upper 100 m, while the major part of the water column (100 to 1300 m) consisted of cold Norwegian Sea Deep Water (θ < 0.5°C, salinity = 34.9), and there was a permanent density gradient between the 2 water masses. The shallow Shetland Shelf station was mixed to the bottom (MLD = bottom = 160 m), was characterized by a uniform water mass of Atlantic Water and remained similar between visits (Fig. 3). The dominating water masses at each of the 3 localities remained consistent throughout the period (the only intrusion of other water masses occurred in the Iceland Basin at 1200 to 1250 m).

Changes in chl *a*, nutrients and DOC:DON ratio

The integrated mean values of chl *a* (mg m^{-3}) within the mixed layer at the 3 stations all showed a gradual increase during the cruise (Table 2, Figs. 3 & 4). Because of the ongoing deep convection at the Iceland Basin and Shetland Shelf stations (from now on referred to as the deep mixed stations), a large fraction of chl *a* was detrained, i.e. mixed well below the photic zone (Fig. 3). The deep mixed stations showed the highest increase in chl *a*, in the Iceland Basin from <0.1 to 0.7 mg m^{-3} during a 30 d period and over the Shetland Shelf from 0.5 to 1.4 mg m^{-3} during a 14 d period. The increase in chl *a* at the deep mixed stations was mainly due to an increase in the >50 µm chl *a* fraction; however, the 10 to 50 µm fraction also increased in the Shetland Shelf (Fig. 4), which comprised up to 50% of the total chl *a* during the last visit. At the more stratified Norwegian Basin, chl *a* was retained within the photic zone (Fig. 3), yet here we observed the smallest increase in chl *a* within the mixed layer, from 0.4 to 0.6 mg chl *a* m^{-3}. The chl *a* fraction <10 µm comprised a major part of total integrated chl *a*, ranging at all stations from 47 ± 25% at the Iceland Basin to 55 ± 39% on the Shetland Shelf and was especially dominant in the Norwegian Basin at 95 ± 7% on average during the study (Fig. 4).

Nutrient concentrations, i.e. NO_3+NO_2, PO_4 and H_4SiO_4, were high throughout the study and homogeneously distributed over the mixed layers (Table 2), with slightly elevated concentrations below the mixed layer (data not shown). Increases in the >50 µm chl *a* fraction were reflected in a slight decrease in H_4SiO_4, from 4.7 to 4.2 µM at the Iceland Basin and from 2.8 to 1.7 µM at the Shetland Shelf, suggesting a net growth of diatoms at these locations. At the deep mixed stations, the carbon:nitrogen (C:N) ratio of the dissolved organic matter (DOM) decreased from 17 to 15 at the Iceland Basin and from 16 to 14 at the Shetland Shelf, i.e. became increasingly rich in nitrogen and closer to the Redfield ratio (C:N ratio of 6.63). There were no clear changes in DOC or DON at the more stratified Norwegian Basin (Table 2). When comparing our study period to the surface chl *a* during the full year of 2012, it is evident that spring bloom has not yet initiated at the deep basins (Daniels et al. 2015). We consider the initial visit to the Iceland Basin to represent winter conditions based on the extremely low chl *a* values (0.06 mg m^{-3}); the remaining sampling occasions are within the pre-bloom phase, while the last visits to the Shetland Shelf represent early bloom conditions, as substantial uptake of nutrients is evident, i.e. H_4SiO_4 no longer in excess (Egge & Aksnes 1992). The defined seasonal stages of the systems are indicated in Figs. 3, 4 & 7.

Succession of phytoplankton

The picophytoplankton community (<2 µm) was dominated by unidentified picoeukaryotes, while the prokaryotic component, *Synechococcus* sp., was considerably less abundant. However, the relative abundance of *Synechococcus* sp. increased during the study at all stations, from 700 to 1600, 2300 to 4700 and 300 to 600 cells ml^{-1} at the Iceland, Norwegian and Shetland stations, respectively (Fig. 5). The nanophytoplankton fraction (2 to 10 µm) was separated into 2 size groups of ESD: 2 to 5 and 6 to 10 µm (Fig. 3A). For conversion to biomass, the diameters of picoeukaryotes, *Synechococcus* sp. and small and large nanophytoplankton were estimated on 7 occasions (mean ESD ± SD, n = 7) to be 1.7 ± 0.4, 1.1 ± 0.4, 4 ± 0.5 and 9 ± 0.7 µm, respectively.

Table 2. Water column characteristics during the study at Iceland Basin, Norwegian Basin and Shetland Shelf stations. Data are given as mean ± SD and n within the mixed layer except chl *a*, for which the integrated mean within the mixed layer is presented (the mean of 3 integrated profiles from each visit). Ratio of the estimated pico- and nanophytoplankton biomass to the measured <10 µm chl *a* fraction (C:chl *a*) is based on linear correlation. DOC concentration and DOC:DON, HNA:LNA bacteria, V:B, bacteria:HNF and picoeukaryotes:HNF ratios are also given. MLD: mixed layer depth; DOC: dissolved organic carbon; DON: dissolved organic nitrogen; HNA: high nucleic acid; LNA: low nucleic acid; V: virus; B: bacteria; HNF: heterotrophic nanoflagellates. –: data not available

Time (2012)	MLD (m)	Photic zone (m)	NO_3+NO_2, PO_4, H_4SiO_4 (µM)	Total chl *a* (mg m^{-3})	Chl *a* >10 µm (%)	Chl *a* >50 µm (%)	C:chl *a*	DOC (µM)	DOC: DON	HNA: LNA bacteria	V:B	V:B below mixed layer	Bacteria: HNF	Pico-eukaryotes: HNF
Iceland Basin														
26–28 Mar Winter	618	147	13, 0.8, 5	0.06 ± <0.1 n = 3	13.1 ± 5.2	4.7 ± 2.8	47 ± 10 (p < 0.005) r^2 = 0.7	51.1 ± 0.4 n = 20	17.2 ± 0.9 n= 6	2.04 ± 1.5 n = 16	8.2 ± 3.1 n = 16	4.4 ± 2.0 n = 6	8000 n = 16	72 n = 16
7–10 Apr Pre-bloom	493	92	12, 0.8, 5	0.4 ± 0.1 n = 3	81.3 ± 14.1	55.5 ± 31.1	21 ± 12 (p = 0.12) r^2 = 0.35	52.4 ± 2.2 n = 18	17.4 ± 2.4 n = 19	2.3 ± 1.9 n = 14	6.1 ± 1.5 n = 16	6.3 ± 1.9 n = 5	8250 n = 16	125 n = 16
18–21 Apr Pre-bloom	492	78	12, 0.8, 5	0.5 ± 0.1 n = 3	53.7 ± 14.6	45.1 ± 19.8	21 ± 6 (p = 0.01) r^2 = 0.6	51.9 ± 1.4 n = 17	14 ± 1.9 n = 18	4.3 ± 0.9 n = 16	2.9 ± 0.6 n = 16	7.3 ± 2.1 n = 6	1797 n = 16	17 n = 16
27–29 Apr Pre-bloom	344	90	12, 0.8, 4	0.7 ± 0.2 n = 3	62.2 ± 12.6	49.2 ± 11.3	11 ± 6 (p = 0.13) r^2 = 0.25	51.9 ± 0.6 n = 16	15.1 ±1.3 n = 16	3 ± 0.6 n = 6	2.6 ± 0.3 n = 12	4.7 ± 0.9 n = 9	3280 n = 16	7.4 n = 16
Norwegian Basin														
30–31 Mar Pre-bloom	43	103	12, 0.8, 5	0.4 ± 0 n = 3	2.9 ± 1.4	0.2 ± 0.7	43 ± 9 (p < 0.005) r^2 = 0.8	51.6 ± 1.4 n = 7	15.6 ± 2.6 n = 7	1.3 ± 1.2 n = 6	4.4 ± 3.4 n = 6	6 ± 0.8 n = 14	6667 n = 7	281 n = 7
13–14 Apr Pre-bloom	37	105	13, 0.8, 5	0.5 ± 0.1 n = 3	8.3 ± 7.6	0.5 ± 0.3	20 ± 6 (p = 0.008) r^2 = 0.6	51.8 ± 0.8 n = 7	18.1 ± 2.2 n = 7	3.3 ± 1.4 n = 7	3.1 ± 0.3 n = 6	5.1 ± 1.04 n = 14	5517 n = 7	70 n = 7
22–25 Apr Pre-bloom	56	86	12, 0.8, 6	0.6 ± 0.1 n = 3	5 ± 2.3	1.0 ± 0.2	39 ± 8 (p < 0.005) r^2 = 0.7	51.3 ± 1.5 n = 18	14.9 ± 1.5 n = 10	4.4 ± 1.9 n = 7	2.5 ± 0.4 n = 7	4.5 ± 0.4 n = 13	3280 n = 7	32 n = 7
Shetland Shelf														
30–31 Mar Pre-bloom	160	87	9.5, 0.6, 2.8	0.5 ± <0.1 n = 3	6.4 ± 1.4	2.3 ± 0.6	47 ± 15 (p = 0.02) r^2 = 0.5	52.5 ± 2.3 = 13 n	16.3 ± 1.9 n = 13	1.4 ± 0.2 n = 0.2	4.7 ± 0.9 n = 13	–	4648 n = 10	21 n = 10
13–14 Apr Early bloom	160	67	8.5, 0.6, 1.7	1.4 ± 0.2 n = 3	55.3 ± 9.3	42.2 ± 6.7	6 ± 1.5 (p = 0.08) r^2 = 0.8	54.3 ± 0.8 n = 6	13.9 ± 1.2 n = 6	2.4 ± 0.2 n = 12	4.3 ± 0.3 n = 14	–	3243 n = 9	5 n = 9

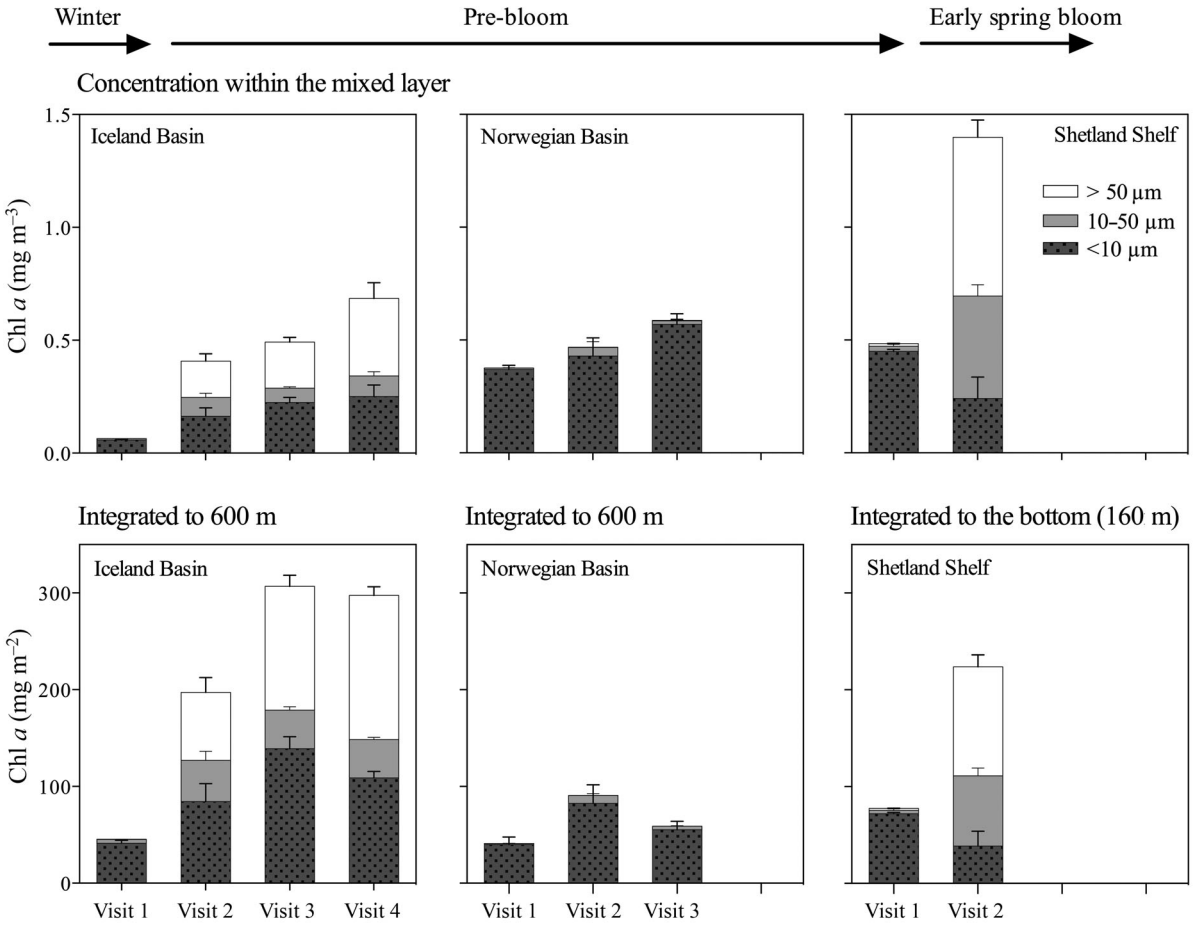

Fig. 4. Size-fractionated chl *a* at the 3 stations over time, shown as mean ± SD (n = 3) of 3 sampled profiles at each visit. Horizontal arrows indicate the seasonal phase. In the upper panels, integrated biomass of chl *a* is divided by mixed layer depth to estimate mean concentration within the mixed layer (mg chl *a* m^{-3}). The integrated biomass (mg chl *a* m^{-2}) to 600 m at the deep stations and to the bottom (160 m) at Shetland Shelf is shown in the lower panels

The abundances of pico- and nanophytoplankton were obtained throughout the mixed layer at all stations (Fig. 5). Maximum abundance was obtained subsurface (below 5 m) at 24 of 27 stations and decreased exponentially below the mixed layer. The average red fluorescence (a measure of chl *a* content) per pico- and nanophytoplankton cell did not change with depth at the deep mixed stations but doubled at the base of the photic zone (±50 m) at the more stratified Norwegian Basin (Fig. 6), suggesting that phytoplankton were able to adapt their chl *a* content to the decrease in irradiance with depth at the more stratified station but not at the mixed stations.

The integrated biomass of small phytoplankton was significantly correlated ($p < 0.05$) with the integrated chl *a* fraction <10 µm. The averaged value of the slopes resulted in a chl *a*:carbon conversion factor of 29 ± 13 (n = 7) for the Iceland Basin and the Norwegian Basin combined. Poor correlations were found for the Shetland Shelf, indicating contributions to the <10 µm chl *a* fraction elsewhere than from the enumerated pico- and nanophytoplankton (Table 2). We found that the <10 µm chl *a* fraction correlated significantly at all stations with the biomass of the pico- and nanophytoplankton converted from flow cytometer counts ($r^2 = 0.58$, $p < 0.0001$, n = 9, slope = 26.6).

The Norwegian Basin station had the highest cell number of pico- and nanophytoplankton within the mixed layer, about twice that of the Iceland Basin and triple that of the Shetland Shelf (Fig. 5). During the first visit to the Norwegian Basin, picoeukaryotes were highly abundant, reaching a maximum of 20 × 10^3 cells ml^{-1}. Despite their small size, this fraction in this case comprised up to 64% of total phytoplankton biomass (the total phytoplankton biomass is calculated from total chl *a* to total phytoplankton carbon by using the conversion factor of 29, described in the

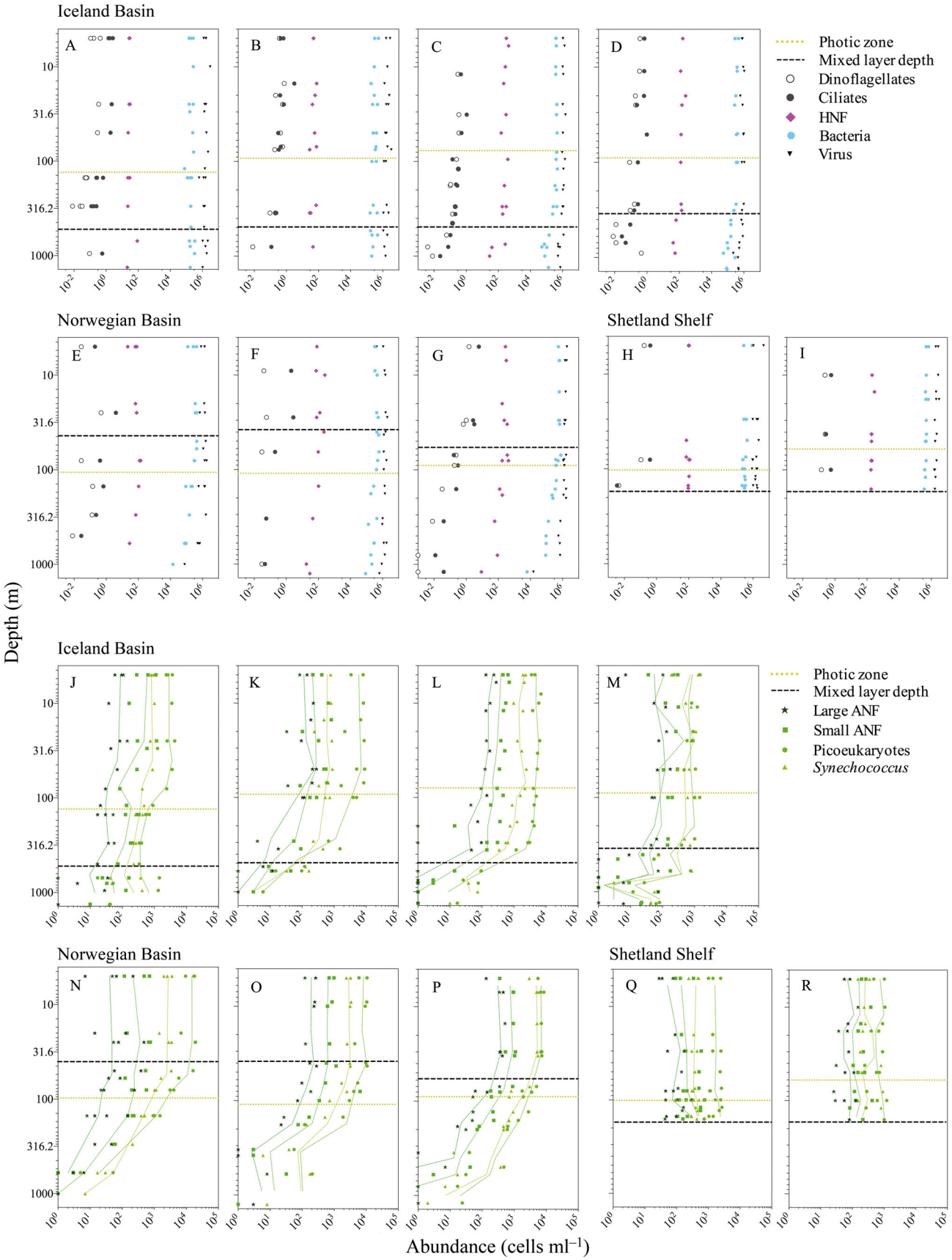
Iceland Basin
Norwegian Basin
Shetland Shelf
Iceland Basin
Norwegian Basin
Shetland Shelf
A
B
C
D
E
F
G
H
I
J
K
L
M
N
O
P
Q
R
Depth (m)
10
31.6
100
316.2
1000
Photic zone
Mixed layer depth
Dinoflagellates
Ciliates
HNF
Bacteria
Virus
Large ANF
Small ANF
Picoeukaryotes
Synechococcus
Abundance (cells ml−1)

Fig. 5. Log-log scale vertical profiles showing the abundance of microorganisms throughout the study (first visit to the left). Triplicate vertical profiles were performed within 20 to 36 h at each visit to the stations. (A–I) Heterotrophic microorganisms: dinoflagellates, ciliates, heterotrophic nanoflagellates (HNF), bacteria and viruses. (J–R) Phototrophic microorganisms: small (>2 to 5 µm) and large (>5 to 10 µm) nanophytoplankton, picoeukaryotes and *Synechococcus* sp. Green and yellow vertical dashed lines (J–R) represent the mean abundance calculated within appropriate depth intervals. Horizontal black dashed lines indicate the depth of the mixed layer; horizontal yellow dashed line marks the photic zone

previous paragraph) (Fig. 7). During subsequent visits to the Norwegian Basin, the abundance of picoeukaryotes decreased gradually to average 6 × 10^3 cells ml^{-1} within the mixed layer, while small nanophytoplankton increased significantly (1-way ANOVA, $p < 0.05$) and became dominant in terms of biomass. Qualitative observations from Lugol's-fixed samples revealed that dominant nanophytoplankton by the end of the period were of the class Cryptophyceae, while diatoms were absent in the Norwegian Basin.

At the deep mixed stations, the increase in the >10 µm chl *a* fraction corresponded well to observations from Lugol's-fixed samples where we observed that larger phytoplankton became more dominant. At the second visit to the Iceland Basin station, we observed a high abundance of *Chaetoceros* spp. (up to 200 cells ml^{-1}) and few *Leptocylindricus* spp., while *Pseudo-nitzschia* spp. became more dominant during the last 2 visits. At the Shetland Shelf station, the large phytoplankton community during the last visit was dominated by the diatoms *Thalassiosira* spp. and *Ditylum brightwellii*. See Daniels et al. 2015 for a more detailed description of the nano- and microphytoplankton community.

Succession of bacteria and virus ratios

In contrast to the photosynthetic plankton and the heterotrophic protists that were distributed evenly only within the mixed layer, bacteria were homogeneously distributed throughout the entire water column, except at the Norwegian Basin station, where a 100-fold decrease in bacterial abundance was evident below 1000 m (Fig. 5). Initially, in late March and early April, the bacterial abundance was low at all stations (2 to 3 × 10^5 cells ml^{-1}) but increased during the following 10 d at all stations to reach around 6 to 7 × 10^5 cells ml^{-1}.

The ratio of HNA:LNA bacteria increased significantly at all stations and was slightly lower below the mixed layer (Table 2, Fig. 8), i.e. fewer active bacteria. Bacteria were the most prominent heterotrophic biomass within the mixed layer (6 ± 3 mg C m^{-3}, n = 27), while viruses comprised the lowest biomass (0.1 ± 0.04 mg C m^{-3}, n = 27). The ratio of

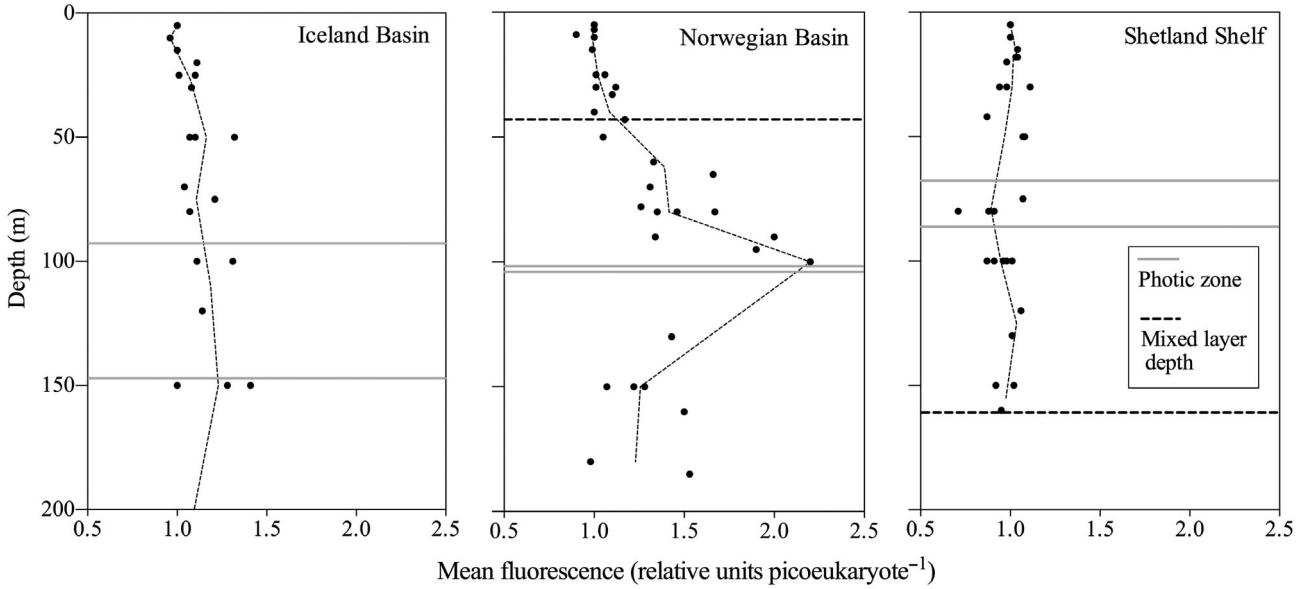

Fig. 6. Changes in mean fluorescence per picoeukaryote normalized by the 5 m value shown for the first 2 visits to each of the 3 stations in the upper 200 m. Horizontal dashed black line defines the mixed layer depth (no black dashed line in Iceland Basin as mixed layer is below 200 m; black dashed line in Shetland Shelf marks the bottom); solid horizontal gray lines mark the photic zone (the deepest photic zones are from the first visit)

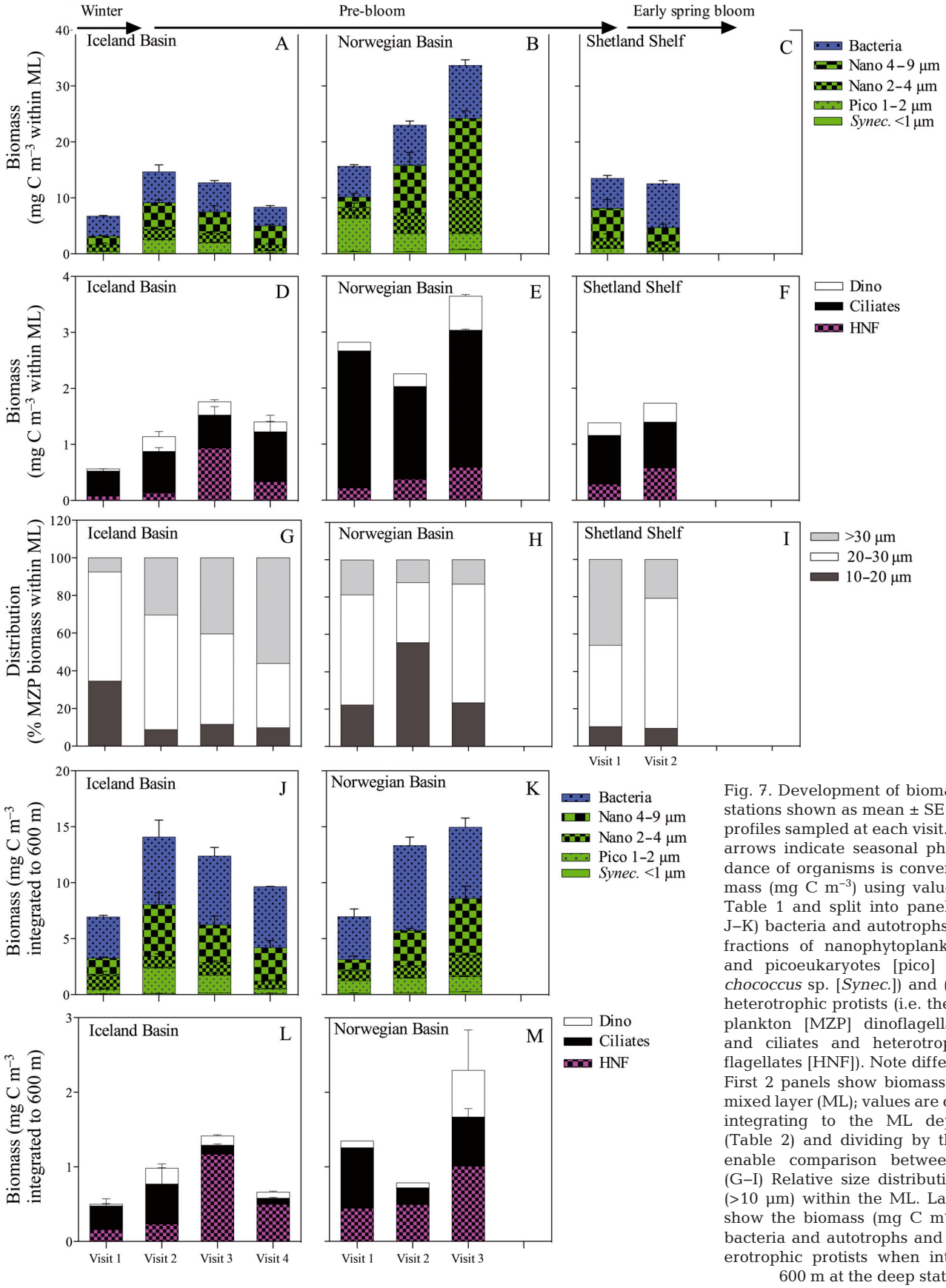

Fig. 7. Development of biomass at the 3 stations shown as mean ± SE (n = 3) of 3 profiles sampled at each visit. Horizontal arrows indicate seasonal phase. Abundance of organisms is converted to biomass (mg C m^{-3}) using values given in Table 1 and split into panels of (A–C, J–K) bacteria and autotrophs (i.e. 2 size fractions of nanophytoplankton [nano] and picoeukaryotes [pico] and *Synechococcus* sp. [*Synec.*]) and (D–F, L–M) heterotrophic protists (i.e. the microzooplankton [MZP] dinoflagellates [dino] and ciliates and heterotrophic nanoflagellates [HNF]). Note different *y*-axis. First 2 panels show biomass within the mixed layer (ML); values are obtained by integrating to the ML depth (MLD) (Table 2) and dividing by the MLD to enable comparison between stations. (G–I) Relative size distribution of MZP (>10 µm) within the ML. Last 2 panels show the biomass (mg C m^{-3}) of (J–K) bacteria and autotrophs and (L–M) heterotrophic protists when integrated to 600 m at the deep stations

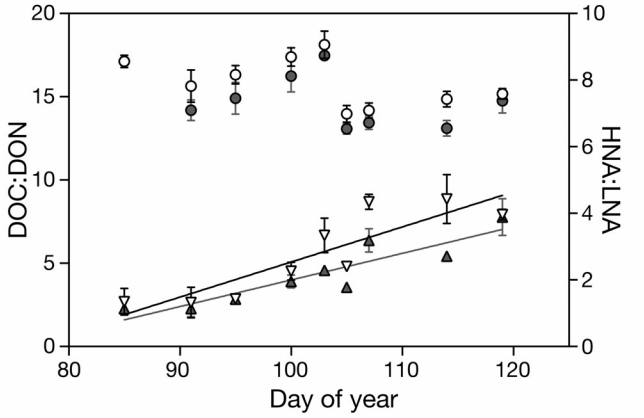

Fig. 8. Carbon:nitrogen ratios (dissolved organic carbon:dissolved organic nitrogen, DOC:DON) of dissolved organic matter within the mixed layer (○) and below the mixed layer (●) and high nucleic acid:low nucleic acid (HNA:LNA) bacteria ratios within the mixed layer (▽) and below the mixed layer (▲) from all 3 stations plotted over time (day of year) during the entire study. Values are given as mean ± SE, n = 6 to 22, and represent the mean within and below the mixed layer (deep) or, for the Shetland Shelf, below 100 m. Linear regressions are given as straight lines for the HNA:LNA ratio within the mixed layer [$f(x) = -7.99 + 0.11x$, $r^2 = 0.83$, $p < 0.005$] and for the HNA:LNA ratio below the mixed layer [$f(x) = -5.99 + 0.08x$; $r^2 = 0.84$, $p < 0.005$]

viruses:bacteria (V:B) decreased at the Iceland Basin and Norwegian Basin stations during the pre-bloom period from 8.2 ± 3.1 and 4.4 ± 3.4 to 2.6 ± 0.3 and 2.5 ± 0.4, respectively, within the upper mixed layer. Below the mixed layer, the V:B ratio was generally higher (Table 2).

HNF

The mean ESD of HNF was 3.2 ± 0.3 µm, n = 170, and did not change during the period. HNF were abundant below the mixed layer, but at depths below 1000 m, they were found in relatively low abundance (23 ± 4 cells ml^{-1}, n = 4) (Fig. 5). Within the upper mixed layer at the first visits to the Iceland Basin and Norwegian Basin stations, the abundance of HNF was low (25 and 48 cells ml^{-1}, respectively) but within 2 to 3 wk increased rapidly 4- to 5-fold. At the first visit to the Shetland Shelf station, the abundance was relatively higher (97 ± 14 cells ml^{-1}) and doubled over the next 10 d (201 ± 31 cells ml^{-1}). In terms of biomass, HNF averaged ~3 ± 1% of their available prey (integrated biomass of bacteria, picoeukaryotes and *Synechococcus*) during the earliest visits to all stations, while later in the study the value increased to ~7 ± 3% of their prey biomass.

MZP

MZP were found to be evenly distributed throughout the mixed layer at all 3 stations (Fig. 5). In the Norwegian and Iceland basins, the abundance of MZP decreased with depth below the mixed layer. At all stations, ciliates contributed on average 73 to 91% of the total MZP biomass, while dinoflagellates made up the remaining part of the biomass (Fig. 7). Integrated MZP biomass (mg C m^{-3}) within the mixed layer was lowest at the Iceland Basin, slightly higher at the Shetland Shelf station and by far highest at the Norwegian Basin (Fig. 7). At the Iceland Basin, MZP integrated biomass increased significantly from the first visit to the 3 later visits (1-way ANOVA, $p < 0.05$). A change in MZP biomass could not be tested for the Norwegian Basin and the Shetland Shelf stations due to lack of replicates, but those samples obtained suggest that there were no marked changes in MZP biomass. The MZP communities at all stations were generally composed of smaller (12 to 30 µm) species (Fig. 7G–I). However, at the Iceland Basin station, the fraction of larger (ESD >30 µm) species increased during the study, and during the last sampling day, 56% of the MZP biomass was composed of individuals with an ESD >30 µm. The Norwegian Basin station was strongly dominated by small cells (ESD <30 µm), contributing >80% of the MZP biomass. Ciliates were dominated by oligotrichs at all stations, but mixotrophic cyclotrichs of the genus *Mesodinium* also contributed substantially to the ciliate biomass, especially at the 3 later visits to the Iceland Basin station. Naked gymnodioid species dominated the dinoflagellate biomass, whereas thecate species made a minimal contribution, <5% of the total MZP biomass (Table 3).

DISCUSSION

Deep mixing enhances accumulation of large phytoplankton

Even during winter, when the sun stays well below the horizon, backscattered light can be detected below 6 m depth at levels high enough to enable photosynthesis (Eilertsen & Degerlund 2010). Backhaus et al. (2003) found presence of a winter stock of phytoplankton within the mixed layer of the Norwegian and Iceland basins and suggested this was enabled by phytoplankton occasionally re-entering the photic zone to harvest light as a result of deep convective mixing during winter. Based on the net increase in

Table 3. Biomass contribution (%) of major groups or species of microzooplankton (dinoflagellates and ciliates) at different visits to the 3 stations

	Iceland Basin				Norwegian Basin			Shetland Shelf	
Visit:	1	2	3	4	1	2	3	1	2
Oligotrichs	87.4	53.5	57.3	62.7	85.9	79.4	83.3	75.6	39.4
Mesodinium spp.	3.7	23.8	18.0	14.8	4.7	8.2	5.7	4.6	33.0
Tintinnids	0.3	0.1	0.3	0.8	1.1	1.1	0.1	0.0	0.1
Gyrodinium spirale	1.0	4.6	5.0	4.5	0.7	1.6	0.5	0.0	1.7
Naked dinoflagellates	6.1	16.1	14.2	14.0	6.8	9.8	10.4	15.8	21.1
Thecate dinoflagellates	1.5	1.9	5.2	3.1	0.8	0.0	0.0	4.1	4.7

chl *a* concentrations, the mixed stations were the most productive, with chl *a* increasing up to 5-fold during the course of our study. In comparison, integrated chl *a* remained roughly the same in the Norwegian Basin, despite an increased day length and excess nutrients (Table 2, Fig. 4). In contrast to Backhaus et al. (2003), who only considered total chl *a* and counts of large phytoplankton, we also considered the community of small phytoplankton behind the chl *a* values.

As the pre-bloom develops, the relative contribution of small cells decreased at the mixed stations, while pico- and nanophytoplankton continued to dominate the phytoplankton biomass at the more stratified Norwegian Basin. This tendency suggests that convective mixing of the water column contributes to the maintenance of large cells such as diatoms in the water column, since the diatoms are otherwise subjected to high sinking losses. Similar selection has been observed in other turbulent systems (Kiørboe 1993). However, large diatoms can also express positive buoyancy under certain conditions, e.g. during light and nutrient saturation the large marine diatom *Ditylum brightwellii* expresses high buoyancy (Waite et al. 1992). Our observations support the fact that increasing light and nutrient-replete conditions could be favourable for large diatom species by further boosting their buoyancy. This is not the case at the Norwegian Basin, however, though light and nutrient conditions are similar, indicating that the convection is more likely an enhancer for diatoms during pre-bloom.

Contribution of picophytoplankton during pre-bloom

Our results demonstrate the quantitative importance of pico- and small nanophytoplankton in the subarctic Atlantic pre-bloom and suggest a new role of small phytoplankton production as an important booster of the late winter microbial heterotrophic community prior to the diatom bloom. The <10 µm chl *a* fraction clearly dominated during the winter and pre-bloom. However, it is not straightforward to draw conclusions on fractionated chl *a*, as small phytoplankton are known to form aggregates (Barber 2007) (and thus may have contributed to the larger fractions of chl *a*) and underestimate the contribution of small phytoplankton. We further document that the more stratified water enables the small phytoplankton to increase their pigment content towards the base of the photic zone (Fig. 6); thereby, using chl *a* as a proxy would overestimate phytoplankton biomass at more stratified stations where phytoplankton are adapted to stable light conditions when compared to the mixed stations. The following discussion is strengthened by being based both on fractionated chl *a* and on the cell counts of small phytoplankton.

Picophytoplankton dominated in numbers throughout the cruise (Fig. 5J–R) but contributed moderately to the integrated phytoplankton biomasses (Fig. 7A–C). However, the fast turnover of picophytoplankton resulted in a larger contribution to phytoplankton production than their small biomass suggests (Agawin et al. 2000). The higher turnover of picophytoplankton was also documented during this study by fractionated primary production measurements, showing the contribution of <10 µm phytoplankton to primary production to be on average 2.7 ± 2.2 times higher than their <10 µm contribution to chl *a* biomass in the Iceland Basin. The same tendency was found at the Norwegian Basin; here, however, the contribution to both chl *a* biomass and the production of large phytoplankton >10 µm was negligible (5 to 10%) throughout the study (Daniels et al. 2015).

The success of picophytoplankton is often assumed to be due to their high affinity for nutrients (Agawin et al. 2000); however, the success of picoeukaryotes during the late winter in high-latitude systems may rather be explained by a high affinity for light com-

pared to larger phytoplankton due to the absence of a cell wall and since the small size of picophytoplankton enables an efficient packaging of photosynthetic pigments inside the cell (Raven 1998). This high affinity for light coupled with their low sinking rates (Kiørboe 1993) position picophytoplankton to respond earlier than other groups to the increase in irradiance in the early spring. This hypothesis is supported by culture experiments with the abundant picophytoplankton *Micromonas*, which were found to have a competitive advantage in both Arctic and subarctic regions due to their relatively high growth rate at low irradiance and low temperature conditions (Lovejoy et al. 2007).

The picophytoplankton community was dominated by picoeukaryote species, whereas the contribution by the prokaryotic compartment, *Synechococcus* sp., was minor. Numeric dominance of eukaryotic picophytoplankton relative to prokaryotes is characteristic for high-latitude waters (Tremblay et al. 2009). A picoeukaryote peak abundance of 20×10^3 cells ml^{-1} was found in the Norwegian Basin, which is comparable to peak abundances reported prior to the bloom in Norwegian coastal waters (Sandaa & Larsen 2006, Bratbak et al. 2011). Tremblay et al. (2009) compared the abundance of picophytoplankton at 10 sites in northern systems during spring, summer and late summer. Our novel observations of picophytoplankton during the period of winter–spring transition are in general higher than those found later in the season.

It is open to dispute whether pico- and small nanophytoplankton are insignificant during the bloom period as found by Joint et al. (1993) or whether they may still comprise a substantial part of the bloom as found by Sherr et al. (2003). As also discussed in Daniels et al. (2015), it is likely that the development we observe during pre-bloom will result in different spring blooms; while the Norwegian Basin spring bloom may continue to be dominated by pico- and small nanophytoplankton, the deep mixed stations are likely to be dominated by diatoms. The composition of phytoplankton during blooms is crucial for zooplankton and the energy transfer to higher trophic levels.

Our initial observations in late March at the Iceland Basin indicate that there are surviving winter stocks of both large and small phytoplankton. The early succession suggests that picoeukaryotes have the greatest advantage earliest in the season with lowest light conditions. Nanophytoplankton remain unchanged in deep mixed waters, whereas the accumulation of large phytoplankton (diatoms) rapidly increases in the deep convective waters of the Iceland Basin and Shetland Shelf (Fig. 4). In the more stratified Norwegian Basin, chl *a* remained in the <10 µm fraction, but within this fraction, there was a clear change from dominance of picophytoplankton to dominance of small nanophytoplankton (Fig. 7). The difference in development is likely caused by the difference in convective mixing, as discussed in the previous section. Moreover, difference in grazing control is likely to play a crucial role, as discussed in the next section.

Heterotrophic protist: top-down control on picophytoplankton?

The heterotrophic protists (HNF and MZP) followed the same homogeneous distribution within the mixed layer as the phytoplankton (Fig. 5); however, whereas MZP decreased exponentially below the mixed layer, HNF showed a more uniform distribution towards the bottom, resulting in a relatively higher biomass when integrated to 600 m (Fig. 7L,M). The highest biomass of heterotrophic protists was found in the more stratified Norwegian Basin, where ciliates dominated the biomass (Fig. 7E). Ciliates also dominated the biomass of heterotrophic protists at the 2 deep mixed stations. However, when considering the higher growth rates of HNF relative to MZP (Hansen et al. 1997), HNF's contribution to heterotrophic protist production may be higher than their biomass suggests. This is supported by incubation experiments conducted during the study with surface water from the Iceland Basin, which showed HNF to have significantly higher growth rates (0.48 ± 0.17 d^{-1}, n = 6) than MZP (0.15 ± 0.05 d^{-1}, n = 3) (K. Riisgaard et al. unpubl.).

The cell numbers of HNF we encountered were in general in the lower end of those observed globally (Sanders et al. 1992) but very similar to those found in Arctic marine systems during the period of winter–spring transition (Vaqué et al. 2008, Iversen & Seuthe 2011). Peak abundances of 300 cells ml^{-1} were observed during our study period. Kuipers et al. (2003) document peak HNF numbers of up to 8000 cells ml^{-1} in the Faroe–Shetland Channel (60 to 62°N) during summer. This suggests that the rapid increase in the abundance of HNF we observed might be sustained through the spring season, thus maintaining a high grazing pressure on bacteria and picophytoplankton. The average diameter of HNF found in this study, 3.2 ± 0.3 µm, agrees with the ≤3 µm obtained by Jürgens & Massana (2008) for 76% of HNF across 4 different

marine systems. HNF with a diameter of 2 to 5 µm have been observed to ingest 1.5 to 2 µm picoeukaryotes and coccoid cyanobacteria (Sherr et al. 1997). It has long been assumed that HNF feed on pico-sized phytoplankton (Fenchel 1982, Azam et al. 1983), yet recent studies on the grazing potential of HNF focus on quantifying bacterivory and neglect the additional portion of carbon taken up via picophytoplankton (Tanaka et al. 1997, Iriarte et al. 2008). They are, however, major grazers of picophytoplankton (Christaki et al. 2001, Sherr & Sherr 2002, Bręk-Laitinen & Ojala 2011), and it remains for future studies to resolve the importance of HNF grazing. We here would suggest splitting the group into large and small HNF to test whether the size groups have different prey-size preferences as speculated by Sherr & Sherr (2002) and Vaqué et al. (2008). Both of these studies suggest that heterotrophic flagellates <5 µm are the main grazers on bacteria, while flagellates >5 µm select for picoeukaryotes. We observe that the decrease in picoeukaryote biomass mirrors the increase in HNF biomass within the mixed layer of the Norwegian Basin and Shetland Shelf (Fig. 7B,C,E,F), also implied by the gradual decreases in bacteria: HNF and picoeukaryote:HNF ratios during prebloom (Table 2). Still, it is impossible to resolve the top-down controls on pico-sized plankton from *in situ* abundances; however, quantifications of HNF grazing are documented through incubation experiments in K. Riisgaard et al. (unpubl.).

Effect of deep mixing on protist grazing

The biomass (mg C m^{-3}) of dinoflagellates and ciliates was low at all sampling stations compared to biomass obtained during spring and summer in the Norwegian Sea (Verity et al. 1993). However, when integrated over the depth of the mixed layer, MZP biomasses are comparable to spring integrated biomasses (300 to 500 mg C m^{-2}) within the mixed layer of the Norwegian Basin and the high Arctic Kongsfjorden (Verity et al. 1993, Seuthe et al. 2011a) and 2- to 3-fold higher than integrated values estimated during the winter–spring transition in the high Arctic Disko Bay (Levinsen et al. 2000). Thus, although MZP concentrations are relatively low, their integrated biomass is significant at all stations.

Ciliates dominated the MZP biomass, with a relative increase in naked and thecate dinoflagellates at the deep mixed Iceland Basin and Shetland Shelf as diatoms became more abundant. The positive relationship between dinoflagellates and diatoms supports the hypothesis that heterotrophic dinoflagellates are important grazers of diatoms (Sherr & Sherr 2007). The Norwegian Basin was dominated (76 to 86%) by oligotrich ciliates throughout the study, which would also be expected with a phytoplankton community composed of mainly small cells. At all 3 stations, large (>30 µm) species became increasingly important at the Iceland Basin and mirrored the increase in large phytoplankton (>50 µm), while the smaller *Mesodinium* spp. became highly abundant at the Shetland Shelf.

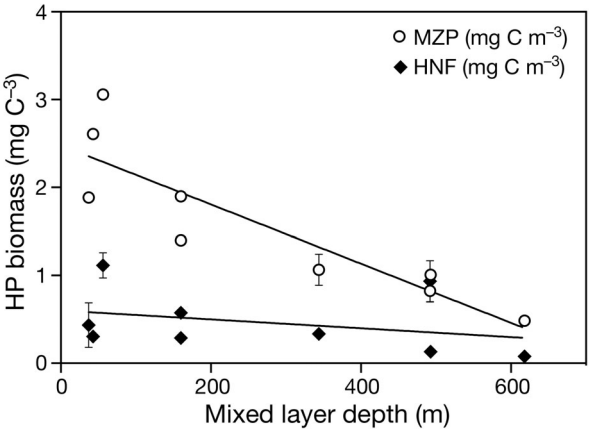

Fig. 9. Biomass of heterotrophic protists (HP) at the 3 stations during the study as a function of mixed layer depth (MLD). Heterotrophic nanoflagellates (HNF) and the sum of heterotrophic dinoflagellates and ciliates (MZP) are shown as average biomass within the MLD (mg C m^{-3}). Linear regression was significant for MZP [$f(x) = -0.0034x + 2.48$, $r^2 = 0.78$, $p < 0.05$] but not for HNF [$f(x) = -0.0005x + 0.6$, $r^2 = 0.10$, $p = 0.39$]

Behrenfeld (2010) and Behrenfeld & Boss (2014) suggested that the higher net increase in phytoplankton biomass during events of deep convection is caused by a dilution of the grazing community. Although the grazers are possibly diluted, as indicated by the homogenously vertical distribution of MZP throughout the mixed layer and a reduction in MZP biomass with increasing mixing depth (Fig. 9), a reduction in numbers of grazers will not necessarily benefit diatoms. Based on the composition of the heterotrophic protists, which were dominated by HNF and ciliates, we argue that a dilution of the grazing community would mainly benefit pico- and nanophytoplankton, whereas diatoms are largely unaffected, the latter because diatoms are unsuitable as prey for HNF and ciliates. Thus, the increase in the >10 µm chl *a* fraction at the mixed stations is more likely to be explained by reduced sinking rates due to deep convection and increased irradiance as the day length increases rather than reduced grazing

pressure from heterotrophic protists being diluted. Alternatively, dilution may have reduced the grazing pressure from other grazers such as copepods (e.g. *Oithona* sp.), which could explain the net growth in large phytoplankton species at the mixed stations.

It must further be considered that the response of mixing is time dependent, i.e. organisms with high growth rates are less affected by dilution. The higher growth rates of HNF, compared to MZP, may be the reason that HNF seem unaffected by deep mixing, while MZP biomass decreases significantly with MLD (Fig. 9). Further, as MZP are also grazers of HNF, the HNF may benefit from the dilution of MZP during deep mixing. When HNF is favoured by deep mixing, the prey of HNF would equally not benefit from deep mixing. Here, we want to underline that the effect of deep mixing in regard to grazing on phytoplankton strongly depends on the size composition of the heterotrophic community.

Controls of bacteria

To our knowledge, there are no previous observations of bacterial abundance during the winter–spring transition in the subarctic North Atlantic. The abundances encountered initially in late March and early April (2 to 3 × 10^5 cells ml^{-1}) are an order of magnitude lower than those observed during the spring bloom in May (47° N, 20° W), where they have been documented to reach 2 × 10^6 cells ml^{-1} (Ducklow et al. 1993) but correspond to observations found during pre-bloom conditions elsewhere in the temperate and Arctic North Atlantic (Bratbak et al. 2011, Seuthe et al. 2011a). It is generally assumed that the growth of heterotrophic bacteria in the winter and pre-bloom phase is substrate limited and the increase in abundance is triggered by DOM excreted from the spring bloom production (Lancelot & Billen 1984, Teeling et al. 2012). Our observations, however, show that bacteria increase in abundance and activity (HNA:LNA ratio) already during pre-bloom. The fact that DOC does not accumulate in the surface layer, despite a net growth of phytoplankton (Fig. 4), infers that the DOC has been taken up by bacteria (Thingstad et al. 1997). Excretion from phytoplankton is generally a very labile carbon source. It has been suggested that smaller phytoplankton excrete relatively more, as the passive excretion is largely due to the passive diffusion of low molecular weight compounds over the cell membrane, which is proportional to the surface:volume ratio and therefore higher for small cells (Bjørnsen 1988), e.g. a study by Malinsky-Rushansky & Legrand (1996) found that picoeukaryotes release 30% of their primary production, while larger nano-sized cells release only 4 to 5%. Therefore, a relatively high contribution to picophytoplankton may benefit bacteria. Our data suggest that bacteria in the deep basins initially were carbon limited, as they responded positively to the growing phytoplankton supply of labile DOC by increasing in numbers within the upper mixed layer between the first and second visits at all stations and expressing higher HNA:LNA ratios (Table 2). Control by bacterivorous grazers and nutrients were assumed to be less important due to low cell numbers of HNF grazers and since NO_3+NO_2 and PO_4 were found in excess.

The C:N ratio of DOM generally decreased during the study from 17.0 to 14.5 in the upper mixed layer and from 15.7 to 13.6 below the mixed layer (Fig. 8), possibly due to grazing and loss of carbon by respiration of the carbon-rich phytoplankton primary production. Labile DOM is characterized by low C:N ratios relative to refractory DOM (Carlson 2002), and therefore the decrease in C:N coincides (however does not correlate significantly, $p = 0.2$) with a significant increase in HNA:LNA bacteria ($r^2 = 0.83$, $p < 0.005$) ratios within the mixed layer as well as below the mixed layer ($r^2 = 0.84$, $p < 0.005$) (Fig. 8), indicating a more actively growing bacterial community (Sherr et al. 2006, Martínez-García et al. 2013). There was, however, an increase in the C:N ratio from the first to the second visit at the Norwegian Basin; this could be explained by a relatively high release of sugars (high C, low N) from picophytoplankton (Giroldo et al. 2005), which dominated at the time.

Decreasing V:B ratio

It is generally assumed that viruses are responsible for 10 to 50% of the bacterial mortality in surface waters and 50 to 100% in environments where grazing protists are low in numbers, e.g. the deep ocean (Fuhrman 1999). The higher the V:B ratio, the higher the expected bacteria mortality induced by strain-specific viruses. During this study, we found a significantly decreasing V:B ratio within the upper mixed layer at all stations (1-way ANOVA, $p < 0.0001$). This was due to an increase in bacteria, which was not mirrored as an increase in viruses. One explanation could be that the strains of bacteria which are the best competitors for the newly produced DOC became dominant over the strains that dominated during the substrate-limited winter, and thus the strain-

specific viruses have not yet evolved for the new strains of dominating bacteria, or that the abundance of bacteria was not sufficient to permit infection by a virus to influence the bacterial community (i.e. a Holling type III or IV reaction). This lag phase by viruses gives the bacterial competition specialists a head start in the pre-bloom phase. Eventually, viruses would be expected to increase in numbers and, according to the killing the winner hypothesis (Thingstad 2000), become a regulating factor for the bacteria community, and the V:B ratio would increase.

Bacteria in deep water benefit from deep mixing

Bacterial abundance in deep oceans is often observed to decline exponentially with depth (Nagata 2000). In contrast, we observed a vertical uniform distribution of bacteria to the bottom (1350 m) of the Iceland Basin, while bacteria decreased significantly towards the bottom at the equally deep Norwegian Basin station (Fig. 5A–G). The relatively high bacterial abundance and increasing HNA:LNA ratio in the deep water of the Iceland Basin is potentially a consequence of deep convective mixing, which has resulted in a homogeneous distribution of bacteria over the water column. This distribution extends below the observed mixed layer at all stations, suggesting that the depth of convective mixing has retreated prior to the program.

Conversely, the homogeneous distribution observed in the heterotrophic organisms is not evidenced in the photosynthetic community at the Iceland and Norwegian basins. The Shetland Shelf station, which was mixed to the bottom by convection during the study period, has a homogeneous distribution of all properties over the entire water column. These observations suggest that the conditions in the convective layer have the potential for a net positive, although low, growth rate as speculated by Backhaus et al. (2003) and Lindemann & St. John (2014). These authors have identified the role of phyto-convection (Backhaus et al. 2003) and below the threshold of critical turbulence resulting in surface blooms (Huisman 1999) in maintaining and fueling production in the convective mixed layer. The cell distributions we observed below the convective depth support the idea of Lindemann & St. John (2014) that cells are potentially detrained from the convective mixed layer, contributing to a pre-spring bloom flux of organic material to depth and here resulting in increased heterotrophic biomass. However, future research is clearly necessary to test this hypothesis.

Our interpretation of the data

This study highlights the importance of the small, fast-growing phytoplankton community as the base of the food web prior to the phytoplankton spring bloom and suggests that deep convection enhances not only phytoplankton accumulation within the mixed layer but also feeds a growing bacterial population below the deep mixed layer. The pre-bloom production feeds a growing community of heterotrophic bacteria and heterotrophic protists and alters the C:N ratio of DOM without depleting the nutrient reservoirs. The subsequent succession and nutrient depletion is caused by larger phytoplankton resistant to small grazers. Our data further suggest that deep mixing reduces grazing on and thus enhances the growth of >10 µm phytoplankton but that the fast-growing HNF are able to keep a tight grazing control on picophytoplankton despite deep mixing. Experimental studies are needed to further assess the coupling between picophytoplankton and their small grazers.

Acknowledgements. The research leading to these results has received funding from the European Union Seventh Framework Programme project EURO-BASIN (ENV.2010.2.2.1-1) under grant agreement no. 264933, ERC grant Microbial Network Organization (MINOS 250254) and the US National Science Foundation (OCE-0752972). The Deep Convection cruise was funded by the Deutsche Forschungsgemeinschaft in a grant to M.S.J. We are very grateful to Dennis A. Hansell for supplying data on TOC and TN. We are also thankful to the crew of the RV 'Meteor' on the Deep Convection Cruise and especially to Françoise Morison and Chris Daniels for good teamwork and for language corrections. Big thanks to Mario Esposito for measuring nutrients during the cruise, and special thanks to Aud Larsen for steadfast flow cytometry assistance. For valuable discussions on an earlier version of the manuscript, we are grateful to Lena Seuthe, Marit Reigstad, Antonio Cuevas and Mathias Middelboe as well the constructive comments of reviewers who helped to improve this manuscript substantially.

LITERATURE CITED

Agawin NSR, Duarte CM, Agustí S (2000) Nutrient and temperature control of the contribution of picoplankton to phytoplankton biomass and production. Limnol Oceanogr 45:591–600

Anderson LG (2002) DOC in the Arctic Ocean. In: Hansell DA, Carlson CA (eds) Biogeochemistry of marine dissolved organic matter. Academic Press, San Diego, CA, p 665–684

Azam F, Fenchel T, Field JG, Gray JS, Meyer-Reil LA, Thingstad F (1983) The ecological role of water-column microbes in the sea. Mar Ecol Prog Ser 10:257–263

Backhaus JO, Wehde H, Hegseth EN, Kämpf J (1999) 'Phyto-convection': the role of oceanic convection in pri-

mary production. Mar Ecol Prog Ser 189:77–92
Backhaus JO, Hegseth EN, Wehde H, Irigoien X, Hatten K, Logemann K (2003) Convection and primary production in winter. Mar Ecol Prog Ser 251:1–14
Barber RT (2007) Picoplankton do some heavy lifting. Science 315:777–778
Behrenfeld MJ (2010) Abandoning Sverdrup's critical depth hypothesis on phytoplankton blooms. Ecology 91: 977–989
Behrenfeld MJ, Boss ES (2014) Resurrecting the ecological underpinnings of ocean plankton blooms. Annu Rev Mar Sci 6:167–194
Bjørnsen PK (1988) Phytoplankton exudation of organic matter: Why do healthy cells do it?. Limnol Oceanogr 33: 151–154
Blindheim J, Østerhus S (2005) The Nordic seas, main oceanographic features. In: Drange H, Dokken T, Furevik T, Gerdes R, Berger W (eds) The Nordic seas: an integrated perspective. AGU Monograph 158, American Geophysical Union, Washington, DC, p 11–37
Børsheim KY, Bratbak G (1987) Cell volume to cell carbon conversion factors for a bacterivorous *Monas* sp. enriched from seawater. Mar Ecol Prog Ser 36:171–175
Braarud BY, Nygaard I (1978) Phytoplankton observations in offshore Norwegian coastal waters between 62°N and 69°N. FiskDir Skr Ser Havunders 16:489–505
Bratbak G, Jacquet S, Larsen A, Pettersson LH, Sazhin AF, Thyrhaug R (2011) The plankton community in Norwegian coastal waters — abundance, composition, spatial distribution and diel variation. Cont Shelf Res 31: 1500–1514
Bręk-Laitinen G, Ojala A (2011) Grazing of heterotrophic nanoflagellates on the eukaryotic picoautotroph *Choricystis* sp. Aquat Microb Ecol 62:49–59
Carlson CA (2002) Production and removal processes. In: Hansell DA, Carlson CA (eds) Biogeochemistry of marine dissolved organic matter. Academic Press, San Diego, CA, p 91–152
Christaki U, Giannakourou A, Wambeke FVANW, Grégori G (2001) Nanoflagellate predation on auto- and heterotrophic picoplankton in the oligotrophic Mediterranean Sea. J Plankton Res 23:1297–1310
Cushing DH (1959) On the nature of production in the sea. Fish Invest Lond Ser II 22:1–40
Daniels CJ, Poulton AJ, Esposito M, Paulsen ML, Bellerby R, St. John M, Martin AP (2015) Phytoplankton dynamics in contrasting early stage North Atlantic spring blooms: composition, succession, and potential drivers. Biogeosciences 12:2395–2409
de Boyer Montégut C, Madec G, Fischer AS, Lazar A, Iudicone D (2004) Mixed layer depth over the global ocean: an examination of profile data and a profile-based climatology. J Geophys Res 109:C12003
Dickson AG, Sabine CL, Christian JR (eds) (2007) Guide to best practices for ocean CO_2 measurements. PICES Special Publication 3. http://cdiac.ornl.gov/ftp/oceans/Handbook_2007/Guide_all_in_one.pdf
Ducklow H, Kirchman D, Quinby H, Carlson C, Dam H (1993) Stock and dynamics of bacterioplankton carbon during the spring bloom in the eastern North Atlantic Ocean. Deep-Sea Res II 40:245–263
Egge JK, Aksnes DL (1992) Silicate as regulating nutrient in phytoplankton competition. Mar Ecol Prog Ser 83: 281–289
Eilertsen HC, Degerlund M (2010) Phytoplankton and light during the northern high-latitude winter. J Plankton Res 32:899–912
Fenchel T (1982) Ecology of heterotrophic microflagellates. IV. Quantitative occurrence and importance as bacterial consumers. Mar Ecol Prog Ser 9:35–42
Fuhrman JA (1999) Marine viruses and their biogeochemical and ecological effects. Nature 399:541–548
Giroldo D, Augusto A, Vieira H (2005) Polymeric and free sugars released by three phytoplanktonic species from a freshwater tropical eutrophic reservoir. J Plankton Res 27:695–705
Hansell DA (2005) Dissolved organic carbon reference material program. EOS Trans. AGU 86(35):318
Hansen PJ, Bjørnsen PK, Hansen BW (1997) Zooplankton grazing and growth: scaling within the 2–2000 µm body size range. Limnol Oceanogr 42:687–704
Hirche H (1996) Diapause in the marine copepod, *Calanus finmarchicus* — a review. Ophelia 44:129–143
Huete-Stauffer TM, Morán XAG (2012) Dynamics of heterotrophic bacteria in temperate coastal waters: similar net growth but different controls in low and high nucleic acid cells. Aquat Microb Ecol 67:211–223
Huisman J (1999) Critical depth and critical turbulence: two different mechanisms for the development of phytoplankton blooms. Limnol Oceanogr 44:1781–1787
Iriarte A, Sarobe A, Orive E (2008) Seasonal variability in bacterial abundance, production and protistan bacterivory in the lower Urdaibai estuary, Bay of Biscay. Aquat Microb Ecol 52:273–282
Irigoien X, Flynn KJ, Harris RP (2005) Phytoplankton blooms: a 'loophole' in microzooplankton grazing impact? J Plankton Res 27:313–321
Iversen KR, Seuthe L (2011) Seasonal microbial processes in a high-latitude fjord (Kongsfjorden, Svalbard): I. Heterotrophic bacteria, picoplankton and nanoflagellates. Polar Biol 34:731–749
Jerlov NG (1968) Optical oceanography. Elsevier, New York, NY
Jespersen AM, Christoffersen K (1987) Measurement of chlorophyll-a from phytoplankton using ethanol as extraction solvent. Arch Hydrobiol 109:445–454
Joint I, Pomroy A, Savidge G, Boyd P (1993) Size-fractionated primary productivity in the northeast Atlantic in May–July 1989. Deep-Sea Res II 40:423–440
Jürgens K, Massana R (2008) Protistan grazing on marine bacterioplankton. In: Kirchman DL (ed) Microbial ecology of the oceans, 2nd edn. John Wiley & Sons, Hoboken, NJ, p 383–441
Kana TM, Glibert PM (1987) Effect of irradiances up to 2000 µE m^{-2} s^{-1} on marine *Synechococcus* WH7803 — I. Growth, pigmentation, and cell composition. Deep-Sea Res 34:479–495
Kiørboe T (1993) Turbulence, phytoplankton cell size and the structure of pelagic food webs. Adv Mar Biol 29:2–61
Koroleff F (1983) Determination of nutrients. In: Grasshoff K, Erhardt M, Kremling K (eds) Methods of seawater analysis. Verlag Chemie, Weinheim, p 125–187
Kuipers B, Witte H, van Noort G, Gonzalez S (2003) Grazing loss-rates in pico- and nanoplankton in the Faroe-Shetland Channel and their different relations with prey density. J Sea Res 50:1–9
Lancelot C, Billen G (1984) Activity of heterotrophic bacteria and its coupling to primary production during the spring phytoplankton bloom in the southern bight of the North Sea. Limnol Oceanogr 29:721–730

Larsen A, Flaten GAF, Sandaa RA, Castberg T and others (2004) Spring phytoplankton bloom dynamics in Norwegian coastal waters: microbial community succession and diversity. Limnol Oceanogr 49:180–190

Lee S, Fuhrman JA (1987) Relationships between biovolume and biomass of naturally derived marine bacterioplankton. Appl Environ Microbiol 53:1298–1303

Levinsen H, Nielsen TG, Hansen BW (2000) Annual succession of marine pelagic protozoans in Disko Bay, West Greenland, with emphasis on winter dynamics. Mar Ecol Prog Ser 206:119–134

Li WKW (1980)Temperature adaptation in phytoplankton: cellular and photosynthetic characteristics. In: Falkowski PG (ed) Primary productivity in the sea. Plenum Press, New York, NY, p 259–279

Li WKW, Dickie PM, Harrison WG, Irwin BD (1993) Biomass and production of bacteria and phytoplankton during the spring bloom in the western North Atlantic Ocean. Deep-Sea Res II 40:307–327

Lindemann C, St John MA (2014) A seasonal diary of phytoplankton in the North Atlantic. Front Mar Sci 37:1–6

Lovejoy C, Vincent WF, Bonilla S, Roy S and others (2007) Distribution, phylogeny, and growth of cold-adapted picoprasinophytes in Arctic seas. J Phycol 43:78–89

Mahadevan A, D'Asaro E, Lee C, Perry MJ (2012) Eddy-driven stratification initiates North Atlantic spring phytoplankton blooms. Science 337:54–58

Malinsky-Rushansky NZ, Legrand C (1996) Excretion of dissolved organic carbon by phytoplankton of different sizes and subsequent bacterial uptake. Mar Ecol Prog Ser 132:249–255

Marie D, Brussaard CPD, Thyrhaug R, Bratbak G, Vaulot D (1999) Enumeration of marine viruses in culture and natural samples by flow cytometry. Appl Environ Microbiol 65:45–52

Martínez-García S, Fernández E, del Valle DA, Karl DM, Teira E (2013) Experimental assessment of marine bacterial respiration. Aquat Microb Ecol 70:189–205

Menden-Deuer S, Lessard EJ (2000) Carbon to volume relationships for dinoflagellates, diatoms, and other protist plankton. Limnol Oceanogr 45:569–579

Mullin MM, Sloan PR, Eppley RW (1966) Relationship between carbon content, cell volume, and area in phytoplankton. Limnol Oceanogr 11:307–311

Murphy J, Riley JP (1962) A modified single solution method for the determination of phosphate in natural waters. Anal Chim Acta 27:31–36

Nagata T (2000) Production mechanisms of dissolved organic matter. In: Kirchman DL (ed) Microbiology of the oceans. Wiley-Liss, New York, NY, p 121–152

Paulsen ML, Riisgaard K, Nielsen TG (2014a) Abundance of bacteria and virus during the Meteor cruise M87/1. PANGAEA, doi:10.1594/PANGAEA.839415

Paulsen ML, Riisgaard K, Nielsen TG (2014b) Abundance of pico- and nanophytoplankton during the Meteor cruise M87/1. PANGAEA, doi:10.1594/PANGAEA.839416

Pomeroy LR (1974) The ocean's food web, a changing paradigm. Bioscience 24:499–504

Porter KG, Feig YS (1980) The use of DAPI for identifying and counting aquatic microflora. Limnol Oceanogr 25: 943–948

Putt M, Stoecker DK (1989) An experimentally determined carbon:volume ratio for marine 'oligotrichous' ciliates from estuarine and coastal waters. Limnol Oceanogr 34: 1097–1103

Raven JA (1998) Small is beautiful: the picophytoplankton. Funct Ecol 12:503–513

Sandaa RA, Larsen A (2006) Seasonal variations in virus-host populations in Norwegian coastal waters: focusing on the cyanophage community infecting marine *Synechococcus* spp. Appl Environ Microbiol 72:4610–4618

Sanders RW, Caron DA, Berninger UG (1992) Relationships between bacteria and heterotrophic nanoplankton in marine and fresh waters: an inter-ecosystem comparison. Mar Ecol Prog Ser 86:1–14

Seuthe L, Iversen KR, Narcy F (2011a) Microbial processes in a high-latitude fjord (Kongsfjorden, Svalbard): II. Ciliates and dinoflagellates. Polar Biol 34:751–766

Seuthe L, Töpper B, Reigstad M, Thyrhaug R, Vaquer-Sunyer R (2011b) Microbial communities and processes in ice-covered Arctic waters of the northwestern Fram Strait (75 to 80°N) during the vernal pre-bloom phase. Aquat Microb Ecol 64:253–266

Sherr EB, Sherr BF (2002) Significance of predation by protists in aquatic microbial food webs. Antonie van Leeuwenhoek 81:293–308

Sherr EB, Sherr BF, Wheeler PA, Thompson K (2003) Temporal and spatial variation in stocks of autotrophic and heterotrophic microbes in the upper water column of the central Arctic Ocean. Deep-Sea Res I 50:557–571

Sherr EB, Sherr BF (2007) Heterotrophic dinoflagellates: a significant component of microzooplankton biomass and major grazers of diatoms in the sea. Mar Ecol Prog Ser 352:187–197

Sherr EB, Sherr BF, Fessenden L (1997) Heterotrophic protists in the central Arctic Ocean. Deep-Sea Res II 44: 1665–1682

Sherr EB, Sherr BF, Longnecker K (2006) Distribution of bacterial abundance and cell-specific nucleic acid content in the northeast Pacific Ocean. Deep-Sea Res I 53:713–725

Søndergaard M, Jensen LM, Ærtebjerg G (1991) Picoalgae in Danish coastal waters during summer stratification. Mar Ecol Prog Ser 79:139–149

Sorokin YI (1977) The heterotrophic phase of plankton succession in the Japan Sea. Mar Biol 41:107–117

Steele JH (1974) The structure of marine ecosystems. Harvard University Press, Cambridge, MA

Sverdrup H (1953) On conditions for the vernal blooming of phytoplankton. J Cons Int Explor Mer 18:287–295

Tanaka T, Fujita N, Taniguchi A (1997) Predator-prey eddy in heterotrophic nanoflagellate-bacteria relationships in a coastal marine environment: a new scheme for predator-prey associations. Aquat Microb Ecol 13:249–256

Taylor JR, Ferrari R (2011) Shutdown of turbulent convection as a new criterion for the onset of spring phytoplankton blooms. Limnol Oceanogr 56:2293–2307

Teeling H, Fuchs BM, Becher D, Klockow C and others (2012) Substrate-controlled succession of marine bacterioplankton populations induced by a phytoplankton bloom. Science 336:608–611

Thingstad TF (2000) Elements of a theory for the mechanisms controlling abundance, diversity, and biogeochemical role of lytic bacterial viruses in aquatic systems. Limnol Oceanogr 45:1320–1328

Thingstad TF, Hagström Å, Rassoulzadegan F (1997) Accumulation of degradable DOC in surface waters: Is it caused by a malfunctioning microbial loop? Limnol Oceanogr 42:398–404

Tremblay G, Belzile C, Gosselin M, Poulin M, Roy S, Tremblay JE (2009) Late summer phytoplankton distribution

along a 3500 km transect in Canadian Arctic waters: strong numerical dominance by picoeukaryotes. Aquat Microb Ecol 54:55–70

Vaqué D, Guadayol Ò, Peters F, Felipe J and others (2008) Seasonal changes in planktonic bacterivory rates under the ice-covered coastal Arctic Ocean. Limnol Oceanogr 53:2427–2438

Verity PG, Langdon C (1984) Relationships between lorica volume, carbon, nitrogen, and ATP content of tintinnids in Narragansett Bay. J Plankton Res 6:859–868

Verity PG, Stoecker DK, Sieracki ME, Nelson JR (1993) Grazing, growth and mortality of microzooplankton during the 1989 North Atlantic spring bloom at 47°N, 18°W. Deep-Sea Res I 40:1793–1814

Waite AM, Thompson PA, Harrison PJ (1992) Does energy control the sinking rates of marine diatoms? Limnol Oceanogr 37:468–477

Williams PJLB (1981) Incorporation of microheterotrophic processes into the classical paradigm of the planktonic food web. Kieler Meeresforsch Sondh 5:1–28

Wood ED, Armstrong FAJ, Rich FA (1967) Determination of nitrate in seawater by cadmium-copper reduction to nitrate. J Mar Biol Assoc UK 47:23–31

Zubkov MV, Sleigh M, Tarran GA, Burkill P, Leakey RJ (1998) Picoplanktonic community structure on an Atlantic transect from 50°N to 50°S. Deep-Sea Res I 45: 1339–1355

Zubkov MV, Burkill PH, Topping JN (2007) Flow cytometric enumeration of DNA-stained oceanic planktonic protists. J Plankton Res 29:79–86

Editorial responsibility: Urania Christaki, Wimereux, France

Submitted: January 13, 2015; Accepted: July 25, 2015
Proofs received from author(s): September 7, 2015